Determinants of coupled transport and uncoupled current by the electrogenic SLC26 transporters

Ehud Ohana,[1,2] Nikolay Shcheynikov,[1,2] Dongki Yang,[1,2] Insuk So,[3] and Shmuel Muallem[1,2]

[1]Epithelial Signaling and Transport Section, Molecular Physiology and Therapeutics Branch, National Institute of Dental and Craniofacial Research, National Institutes of Health, Bethesda, MD 20892
[2]Department of Physiology, University of Texas Southwestern Medical Center, Dallas, TX 75390
[3]Department of Physiology and Biophysics, Seoul National University College of Medicine, Seoul 110-799, Korea

Members of the SLC26 family of anion transporters mediate the transport of diverse molecules ranging from halides to carboxylic acids and can function as coupled transporters or as channels. A unique feature of the two members of the family, Slc26a3 and Slc26a6, is that they can function as both obligate coupled and mediate an uncoupled current, in a channel-like mode, depending on the transported anion. To identify potential features that control the two modes of transport, we performed in silico modeling of Slc26a6, which suggested that the closest potential fold similarity of the Slc26a6 transmembrane domains is to the CLC transporters, despite their minimal sequence identity. Examining the predicted Slc26a6 fold identified a highly conserved glutamate (Glu^-; Slc26a6(E357)) with the predicted spatial orientation similar to that of the CLC-ec1 E148, which determines coupled or uncoupled transport by CLC-ec1. This raised the question of whether the conserved Glu^- in Slc26a6(E357) and Slc26a3(E367) have a role in the unique transport modes by these transporters. Reversing the Glu^- charge in Slc26a3 and Slc26a6 resulted in the inhibition of all modes of transport. However, most notably, neutralizing the charge in Slc26a6(E357A) eliminated all forms of coupled transport without affecting the uncoupled current. The Slc26a3(E367A) mutation markedly reduced the coupled transport and converted the stoichiometry of the residual exchange from $2Cl^-/1HCO_3^-$ to $1Cl^-/1HCO_3^-$, while completely sparing the current. These findings suggest the possibility that similar structural motif may determine multiple functional modes of these transporters.

The Journal of General Physiology

INTRODUCTION

Transepithelial Cl^- absorption and HCO_3^- secretion is critical for the function of all epithelial tissues. HCO_3^- is the mobile physiological pH buffer that protects cells from fast and local changes in intracellular pH (Boron, 2004; Casey et al., 2010). In the epithelial mucosal layer, HCO_3^- maintains acid–base balance and facilitates ion and macromolecule solubilization in the secreted fluids, in particular, mucins and proteolytic enzymes (Allen et al., 1993). Aberrant HCO_3^- secretion is associated with many epithelial and inflammatory diseases, such as cystic fibrosis (Durie, 1989), congenital chloride diarrhea (Höglund et al., 1996), pancreatitis (Baron, 2000; Ko et al., 2010), and Sjögren's syndrome (Almståhl and Wikström, 2003). HCO_3^- secretion is fueled by the inward electrochemical gradient for Cl^- that is used by Cl^-/HCO_3^- exchangers to mediate HCO_3^- efflux at the luminal membrane. The main epithelial Cl^-/HCO_3^- exchangers at the luminal membrane are the Slc26a3, Slc26a4, and Slc26a6 members of the SLC26 transporters family (Dorwart et al., 2008).

The SLC26 family consists of 10 members that show diverse transport modes and ion specificity (Dorwart et al., 2008). Mutations in several members are associated with disease states. For example, mutations in SLC26A4 are associated with Pendred syndrome, assumed to be caused by abnormal I^- transport (Everett et al., 1997). Slc26a4 also affects systemic acid–base balance and inner endolymph pH (Wangemann et al., 2007; Wall and Pech, 2008) because it functions as a coupled electroneutral $Cl^-/I^-/HCO_3^-$ exchanger (Shcheynikov et al., 2008). Mutations in SLC26A3 result in congenital Cl^- diarrhea, an autosomal recessive disorder caused by impaired intestinal Cl^- absorption (Höglund et al., 1996). Slc26a3 functions as a coupled electrogenic $2Cl^-/1HCO_3^-$ exchanger (Shcheynikov et al., 2006). Slc26a6 is an electrogenic multifunctional transporter that mediates $1Cl^-/2HCO_3^-$ exchange (Shcheynikov et al., 2006). Slc26a6 also mediates $Cl^-/oxalate^=$ and $Cl^-/formate^-$ exchange (Knauf et al., 2001; Jiang et al., 2002; Xie et al., 2002). Deletion of Slc26a6 in mice causes hyperoxaluria and Ca-oxalate urolithiasis (Jiang et al., 2006).

A unique feature of Slc26a3 and Slc26a6 is that they can function simultaneously as obligate Cl^-/HCO_3^- exchangers and can conduct anionic currents

E. Ohana and N. Shcheynikov contributed equally to this paper.
Correspondence to Shmuel Muallem: shmuel.muallem@nih.gov
Abbreviation used in this paper: TMD, transmembrane domain.

The Rockefeller University Press $30.00
J. Gen. Physiol. Vol. 137 No. 2 239–251
www.jgp.org/cgi/doi/10.1085/jgp.201010531

(Shcheynikov et al., 2006). This is an unusual feature of coupled transporters and resembles the defined case of several of the CLC transporters (Jentsch, 2008). The seminal finding in the case of the CLCs is that the bacterial CLC-ec1 functions as a $2Cl^-/H^+$ exchanger (Accardi and Miller, 2004). The available crystal structures of bacterial CLC-ec1, CLC-st (Dutzler et al., 2002), and now of a eukaryotic CLC (Feng et al., 2010) indicate that coupling is determined by a highly conserved glutamate (E148 in CLC-ec1) in transmembrane domain (TMD) Fα. Neutralization of the charge resulted in uncoupled Cl^- current activity by CLC-ec1 (Accardi and Miller, 2004) and the eukaryotic CLC (Feng et al., 2010). Similar activity was then reported for CLC3 (Matsuda et al., 2008), CLC4, and CLC5 (Picollo and Pusch, 2005; Scheel et al., 2005). However, a difference between the SLC26 and CLC transporters is that the coupled and uncoupled transport modes are mediated by the native SLC26 transporters, whereas mutation of the Glu^- in the conductive pathway is required to observe the Cl^- current by the CLC transporters.

An important question is what property of the SLC26 transporters determines the mode of transport. To address this question, we performed in silico modeling of Slc26a6 to identify features that may affect its transport properties. The closest meaningful architecture to that of Slc26a6 based on 3-D structural analysis was with the bacterial CLC-ec1. This was somewhat surprising because there is very limited sequence similarity between Slc26a6 and CLC-ec1. The derived Slc26a6 model identified a highly conserved glutamate (E357) residue at the predicted TMD 9 that is spatially oriented similarly to the corresponding glutamate (E148) residue of CLC-ec1. The equivalent glutamate (Glu^-) in Slc26a3 is E367. We mutated these Glu^- to neutralize or reverse the charge and asked whether the conserved Glu^- determines Slc26a3 and Slc26a6 mode of transport. We report that reversing the Glu^- charge in both Slc26a3 and Slc26a6 resulted in the inhibition of all the transport modes. However, most notably, neutralizing the charge in Slc26a6(E357A) eliminated all forms of coupled transport and augmented the uncoupled current. Similar mutation in Slc26a3(E367A) reduced the coupled transport and converted the stoichiometry of the residual exchange from $2Cl^-/1HCO_3^-$ to $1Cl^-/1HCO_3^-$, while sparing the anionic currents. These findings reveal the central role of the conserved Glu^- in determining the SLC26 transporter properties and raise the possibility of a similar role of the conserved Glu^- in coupled and uncoupled transport by the CLC and SLC26 transporters.

MATERIALS AND METHODS

Computer structure prediction and protein modeling

The mouse slc26a6 protein sequence (NCBI Protein database accession no. NP_599252.2) was submitted to the 3D-Jury metaserver using default settings (Ginalski et al., 2003). The software suggested CLC-ec1 as a homologue, with a Jscore of 51.5. The MaxSprout software (Holm and Sander, 1991) was subsequently used to generate a protein backbone and side chains based on the C-α trace provided by 3D-Jury. The final model was generated using PyMol software (DeLano Scientific LLC). Further details are given in the Results.

Solutions

For experiments in oocytes, the standard HEPES-buffered ND96 medium contained (in mM): 96 NaCl, 2 KCl, 1.8 $CaCl_2$, 1 $MgCl_2$, and 5 HEPES, pH 7.5. The HCO_3^--buffered solution contained (in mM): 71 NaCl, 25 $NaHCO_3^-$, 2 KCl, 1.8 $CaCl_2$, 1 $MgCl_2$, and 5 HEPES-Na, pH 7.5. Cl^--free medium was prepared by replacing Cl^- with gluconate and using Ca^{2+} cyclamate and $MgSO_4$. HCO_3^--buffered solutions were gassed with 5% CO_2 and 95% O_2. NO_3^- and SCN^- solutions were prepared by substituting equimolar concentrations of Cl^- in Cl^--free solutions with either NO_3^- or SCN^-. The whole cell current in HEK cells was measured with pipette solution containing (in mM) 140 KCl, 1 $MgCl_2$, 2 EGTA, 5 ATP, and 10 HEPES, pH 7.3 with Tris, or the same solution in which KCl was replaced with K^+ gluconate. The bath solution was composed of (in mM): 145 NaCl, 1 $MgCl_2$, 1 $CaCl_2$, 10 HEPES, pH 7.4 with NaOH, and 10 glucose. Solutions containing SCN^- or NO_3^- were prepared by isosmotic replacement of NaCl with the respective salts and using $MgSO_4$ and $Ca(OH)_2$.

cRNA preparation

The mouse Slc26a3 (available from GenBank/EMBL/DDBJ under accession no. NM_021353.2) in pXBG-ev1 and mouse Slc26a6 (accession no. NM_134420.4) in pSport-6 clones were the same as those used in previous studies (Shcheynikov et al., 2006). For cRNA preparation, the clones were linearized with NotI and used to transcribe cRNA with mMessage mMachine T3 and Sp6 kits (Applied Biosystems), respectively. Mutants of Slc26a6 and Slc26a3 were generated by a site-directed mutagenesis kit (Agilent Technologies) and verified by nucleotide sequencing.

Biotinylation and Western blot analysis

Transfected cells were washed once with 1× PBS on ice and incubated with EZ-Link Sulfo-NHS-SS-Biotin (0.5 mg/ml; Thermo Fisher Scientific) for 30 min on ice. The biotin was quenched with 50 mM glycine on ice for 3 × 5 min. Lysates were prepared with lysis buffer containing 1× PBS, 1 mM $NaVO_3$, 10 mM Na-pyrophosphate, 50 mM NaF, pH 7.4, and 1% Triton X-100. 200 µl of 1:1 slurry of immobilized avidin beads (Thermo Fisher Scientific) was added to 900 µg of protein in 1 ml of cell extract and incubated overnight. Beads were washed 3 × 10 min with binding buffer, and proteins were released with 100 µl of SDS-loading buffer. 30 µl of the extracts was loaded onto 4–12% Tris-glycine SDS-PAGE gels. Gels were transferred onto PVDF membrane and probed with anti-Slc26a6 polyclonal antibodies diluted at 1:1,000 or anti-GAPDH polyclonal antibody (Abcam) diluted at 1:5,000. Membranes were then incubated with a secondary donkey anti–rabbit IgG (H+L)–horseradish peroxidase conjugate antibody (The Jackson Laboratory) diluted at 1:5,000 (1 h at 25°C). The input represents 2% of the total protein used for the biotinylation assay.

Xenopus laevis oocyte preparation

Oocytes were isolated by partial ovariectomy of anaesthetized female *Xenopus* and treated by collagenase (collagenase B; Roche), as described previously (Ko et al., 2002). Stage V–VI oocytes were injected with 10 ng cRNA using glass micropipettes and a microinjection device (Nanoliter 2000; World Precision Instruments) in a final volume of 27.6 nl. Oocytes were incubated at 18°C in ND96 supplemented with 2.5 mM

pyruvate and antibiotics, and were studied 72–144 h after injection of cRNA.

Voltage, current, pH, and Cl^- measurement in oocytes

Current and voltage recordings were performed at room temperature with two-electrode voltage clamp, as described previously (Ko et al., 2002). Current, voltage, pH_i, and Cl^-_i concentrations were measured as described previously (Shcheynikov et al., 2006). In brief, currents were recorded using amplifier (Warner Instrument Corporation) and digitized via an A/D converter (Digidata 1322A; Axon Instruments, Inc.). Data were analyzed using the Clampex 8.1 system (Axon Instruments, Inc.). Ion-selective microelectrodes were fabricated from thin-walled borosilicate glass capillaries (Warner Instrument Corporation). The pipettes were pulled (PP-830 puller; Narishige) in a two-step program to yield a rapid taper and tip diameter of 2–4 µm. The electrodes were vapor silanized for 12–16 h at room temperature with a 10:1 mixture of carbon tetrachloride-bis(dimethylamino)dimethyl silane. The tips were filled with 0.5 µl of H^+ or Cl^- exchanger resin (hydrogen ionophore I, cocktail B [Sigma-Aldrich]; Cl^--sensitive liquid ion exchanger 477913 [Corning]). The electrodes were backfilled with a 3-M KCl solution.

Because the ion-selective microelectrodes respond to ionic activity and to membrane potential, the membrane potential was measured with electrodes fitted with an Ag-AgCl wire attached to a high-impedance probe of a two-channel electrometer (FD-223; World Precision Instruments). One channel was used for ion-sensitive measurement and another was used to record or control the membrane potential. The junction potential was <2 mV and was not corrected. The pH and Cl^- signals were extracted by subtracting the membrane potential signal from the ion-selective electrodes signal using Origin software (version 8.0; OriginLab). For simultaneous measurement of pH_i and Cl^-_i in oocytes, a three-electrode method was used as described previously (Shcheynikov et al., 2006). Calibration of the ion-selective electrodes was as performed before and after each measurement. The Cl^- microelectrode slope was ∼56 mV per 10-fold change in Cl^- concentration. The slope of the pH electrodes was between 56 and 57 mV (pH unit)$^{-1}$. The Cl^- electrode was used to record intracellular NO_3^- and SCN^-. The electrode has 10- and 1,000-fold higher sensitivity to NO_3^- and SCN^-, respectively. Therefore, results with these anions are plotted relative to their respective controls.

Current measurement in HEK cells

HEK293 cells were maintained in Dulbecco's modified Eagle's medium supplemented with 10% fetal bovine serum. 1 d after plating, cells were transfected with Lipofectamine 2000 (Invitrogen) and used for current recording 24 h later (Yang et al., 2009). The whole cell configuration of the patch clamp technique was used to measure the current in control and Slc26a6-transfected HEK293 cells, as described previously (Shcheynikov et al., 2006). The average pipette resistance was 3–5 MΩ when filled with an intracellular solution. Currents were recorded using a patch clamp amplifier (Axopatch 200A; Axon Instruments, Inc.) at a holding potential of 0 mV, digitized at 2 kHz, and filtered at 1 kHz. I-Vs were obtained by the application of −100 to +100 mV, with 100-ms voltage RAMPs every 5 s from a holding potential of 0 mV. Current recording and analysis were performed with the Clampex 8.1 software.

Online supplemental material

Fig. S1 shows the effect of HCO_3^- on the current mediated by Slc26a6. Fig. S2 shows the predicted secondary structure of Slc26a6, and Fig. S3 shows the conservation of glutamate in the putative SLC26 pores. Figs. S1–S3 are available at http://www.jgp.org/cgi/content/full/jgp.201010531/DC1.

RESULTS

Coupled and uncoupled transport modes by Slc26a6

In a previous study, we showed that Slc26a6 functions as a coupled $1Cl^-/2HCO_3^-$ exchanger (Shcheynikov et al., 2006). This is also demonstrated in Fig. 1 A, which shows the simultaneous measurement of intracellular Cl^- (Cl^-_i), intracellular pH (pH_i), which is translated to intracellular HCO_3^- ($HCO_3^-_i$), and the membrane potential in oocytes expressing Slc26a6 and bathed in HCO_3^--buffered solution. The removal of external Cl^- (Cl^-_o) resulted in Cl^- efflux, HCO_3^- influx, and a large hyperpolarization. A new mode of Slc26a6-mediated transport is shown in Fig. 1 B, which is uncoupled, channel-like anion current. Oocytes were perfused with HEPES-buffered media in which Cl^- was replaced with NO_3^- or SCN^-. This resulted in a robust NO_3^- and SCN^- currents. The relative current mediated by Cl^-, NO_3^-, and SCN^- in the same oocytes is illustrated in Fig. S1 A.

Slc26a6 also transports the single-charge carboxylic acid formate (Knauf et al., 2001; Jiang et al., 2002; Xie et al., 2002) and the double-charged oxalate (Jiang et al., 2002; Xie et al., 2002). Demonstrating transport of these anions by Slc26a6 relied mainly on isotopic fluxes that do not always distinguish between net and exchange fluxes. In addition, the exact coupling of the acids to Cl^- and the mode of transport, in particular for formate, have not been completely resolved. Fig. 1 (C and D) show tight coupling of formate$^-$/Cl^- exchange and the electroneutrality of the exchange. Fig. 1 C shows that the removal of Cl^-_o in oocytes expressing Slc26a6 and bathed in HEPES-buffered medium caused large hyperpolarization as a result of charge distribution (top trace) that is followed by minimal Cl^- efflux. As can be seen in the Cl^- trace, Slc26a6 mediates $1Cl^-_i/2OH^-_o$ exchange, but the exchange is very slow. Hence, when Cl^-_o is removed, the $1Cl^-_i/2OH^-_o$ stoichiometry must result in OH^- distribution that leads to the hyperpolarization. When 10 mM formate$^-$ is included in the Cl^--free medium, the hyperpolarization is largely reversed, but now there is a marked activation of Cl^- efflux as a result of formate$^-$/Cl^- exchange. The removal of formate$^-$ resulted in hyperpolarization and inhibition of Cl^- efflux, and the readdition of formate$^-$ depolarized the oocytes and initiated Cl^- efflux. In Fig. 1 D, the membrane potential was switched from a holding potential of −20 to −80 mV, resulting in ∼0.3 µA of inward current, mostly a result of Cl^-_o/OH^-_i exchange, as evident from its elimination by the removal of Cl^-_o. The addition of 10 mM formate$^-$ had no effect on the current in the presence of Cl^-_o and did not generate a significant current when added to oocytes bathed in Cl^--free medium. The small apparent inward current in Cl^--free medium is likely a result of partial reduction in the Cl^-/OH^- exchange because of the engagement of part of Slc26a6 transporters in electroneutral Cl^-/formate exchange. Hence, the

Slc26a6-mediated formate$^-$ transport is not associated with a change in a membrane potential or a current, consistent with an electroneutral formate$^-$/Cl$^-$ exchange at a 1:1 ratio.

Similar measurement with oxalate$^=$ in Fig. 1 E shows that the addition of oxalate$^=$ results in a large hyperpolarization (top trace) and Cl$^-$ efflux (bottom trace). The membrane potential decayed as the oocytes were depleted of Cl$^-$ and accumulated oxalate$^=$. The removal of oxalate$^=$ halted the change in membrane potential and Cl$^-$ efflux. The readdition of Cl$^-$ resulted in transient depolarization and in Cl$^-$ influx into the Cl$^-$-depleted oocytes. These properties are consistent with the oxalate$^=$/Cl$^-$ exchange ratio of 1:1, and the electrogenicity of the process is a result of the two negative charges of oxalate$^=$. The measurement of Cl$^-$ efflux at 1, 5, and 10 mM formate$^-$ and oxalate$^=$ shows that the fluxes do not saturate, even at 10 mM (not depicted). Yet, the rate of Cl$^-$ efflux evoked by 10 mM formate$^-$ and 1 mM oxalate$^=$ are comparable (Fig. 1 F). This suggests that Slc26a6 transports oxalate$^=$ better than formate$^-$.

The NO_3^- and SCN$^-$ currents stand out as uncoupled fluxes mediated by Slc26a6. To provide additional evidence for the uncoupled, conductive nature of the currents, in Fig. S1 (B and C) we show the effect of HCO_3^- on the NO_3^- or SCN$^-$ currents. We also show the changes in pH_i with NO_3^-. It was not possible to determine the effect of replacing Cl^-_o with SCN$^-$ on pH_i because several batches of the pH resin tested responded to SCN$^-$. Replacing Cl$^-$ with NO_3^- resulted in small acidification in HCO_3^--buffered but not in HEPES-buffered medium, probably because of a minimal $NO_3^-{}_o$/$HCO_3^-{}_i$ exchange. Hence, with NO_3^- the exchange

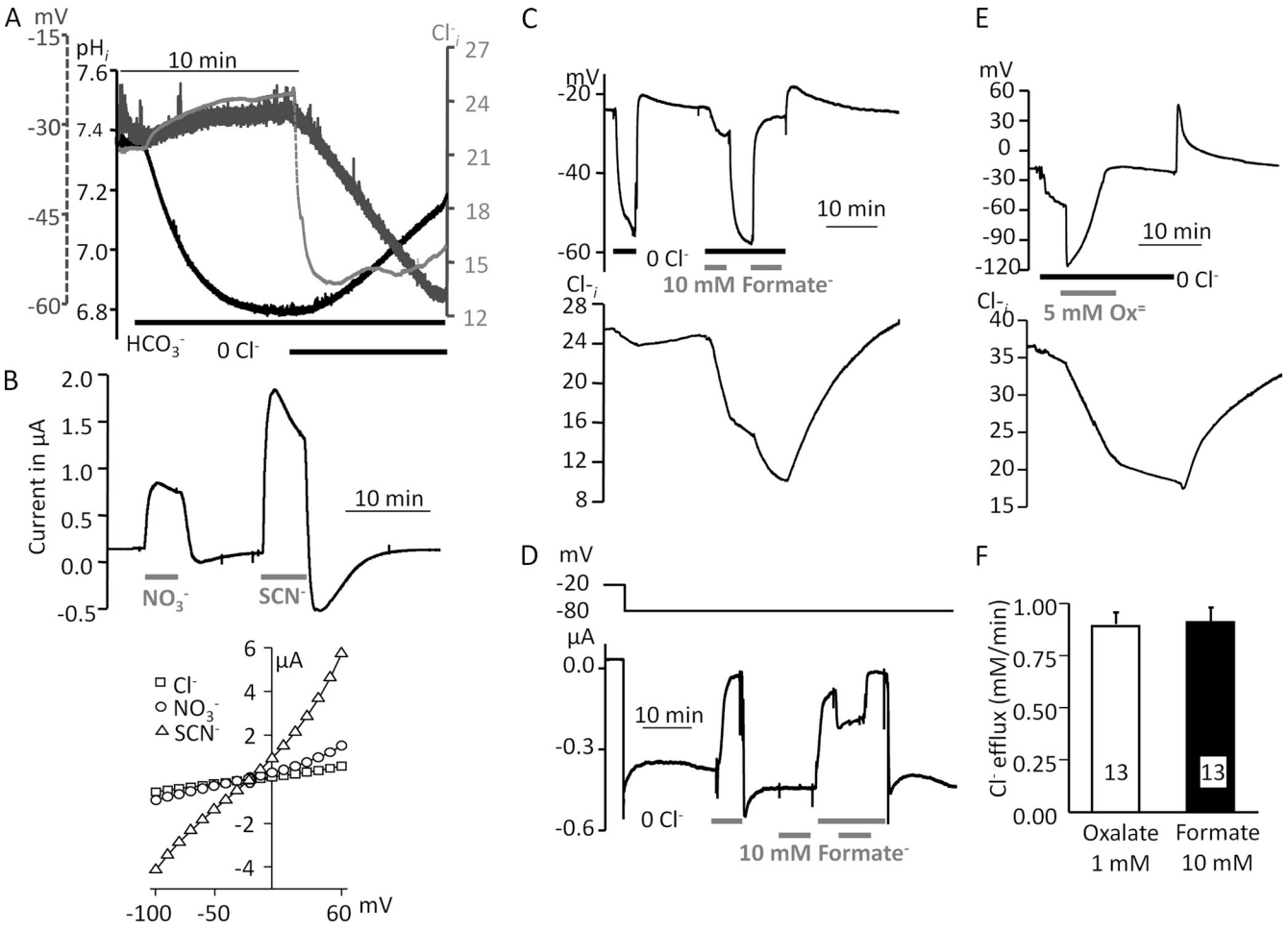

Figure 1. The multiple transport modes of Slc26a6. All experiments are with oocytes expressing wild-type Slc26a6. (A) The simultaneous measurement of membrane potential (light gray trace), pH_i (dark trace), and $[Cl^-]_i$ (gray trace). (B) Measurement of the NO_3^- and SCN$^-$ currents in oocytes held at 0 mV, and typical I-Vs obtained with Cl$^-$, NO_3^-, and SCN$^-$. The I-Vs were obtained after a 5-min incubation with the respective anions to allow uptake of NO_3^- and SCN$^-$ to measure their inward current. (C and E) $[Cl^-]_i$ and membrane potential measurements were used to monitor Cl$^-$/formate$^-$ (C) and Cl$^-$/oxalate$^=$ (E) exchange. (D) Cl$^-$ current in the presence and absence of 10 mM formate was measured at a holding membrane potential of −80 mV by altering bath Cl$^-$. (F) The rates of Cl$^-$ transport in the presence of 1 mM oxalate$^=$ and 10 mM formate$^-$. Results similar to those in A, B, and D were obtained in at least five experiments. Results in F are given as mean ± SEM of the number of experiments listed in the columns.

process is still operating at high rates, even though the uncoupled current is activated. Importantly, HCO_3^- has minimal effect on the NO_3^- and SCN^- currents, and thus, most of the currents must be uncoupled and therefore conductive. If the current was by a coupled mechanism, it should have been strongly increased by HCO_3^- because HCO_3^- markedly increases the Slc26a6-mediated exchange (Shcheynikov et al., 2006). We reported similar properties for the NO_3^- and SCN^- currents mediated by Slc26a3 (Shcheynikov et al., 2006).

To establish further the uncoupled current and determine the anion selectivity of Slc26a6, the whole cell current mediated by Slc26a6 was then measured in HEK cells. Fig. 2 A shows that replacing external Cl^- with NO_3^- or SCN^- at a holding potential of 0 mV resulted in an outward current that was approximately three times larger with SCN^- than with NO_3^-. Fig. 2 (B and D) shows that with 150 mM Cl^-_i, the application of external NO_3^- and SCN^- shifted the reversal potential (Erev) to more negative values, indicating selectivity in the order of $SCN^- > NO_3^- > Cl^-$ for Slc26a6. The SCN^- current persisted in the absence of intracellular Cl^- (Fig. 2 C), which resulted in Erev shift to -40.3 ± 4.0 ($n = 3$; Fig. 2 D). Moreover, the SCN^- current time course in Fig. 2 E and the I-V in Fig. 2 F measured in oocytes expressing Slc26a6 show that the outward current is observed upon the addition of SCN^- to the bath, whereas the inward current develops slowly because of the slow SCN^-_o/Cl^-_{in} exchange and SCN^- accumulation in the oocytes. As SCN^- accumulates, the reversal potential shifted toward the 0 mV. If the SCN^- current was a result of coupled exchange, and the initial large outward current was a result of SCN^-_o/Cl^-_{in} exchange, the current should have been reduced with time because of exhaustion of intracellular Cl^-. This is clearly not the case. Hence, the results in Fig. 2 show that the currents are uncoupled anionic fluxes.

Collectively, the results described in Figs. 1, 2, and S1 indicate that Slc26a6 has multiple transport modes: (a) it can act as a Cl^--coupled exchanger that mediates an electrogenic efflux of either HCO_3^- or oxalate$^=$; (b) it

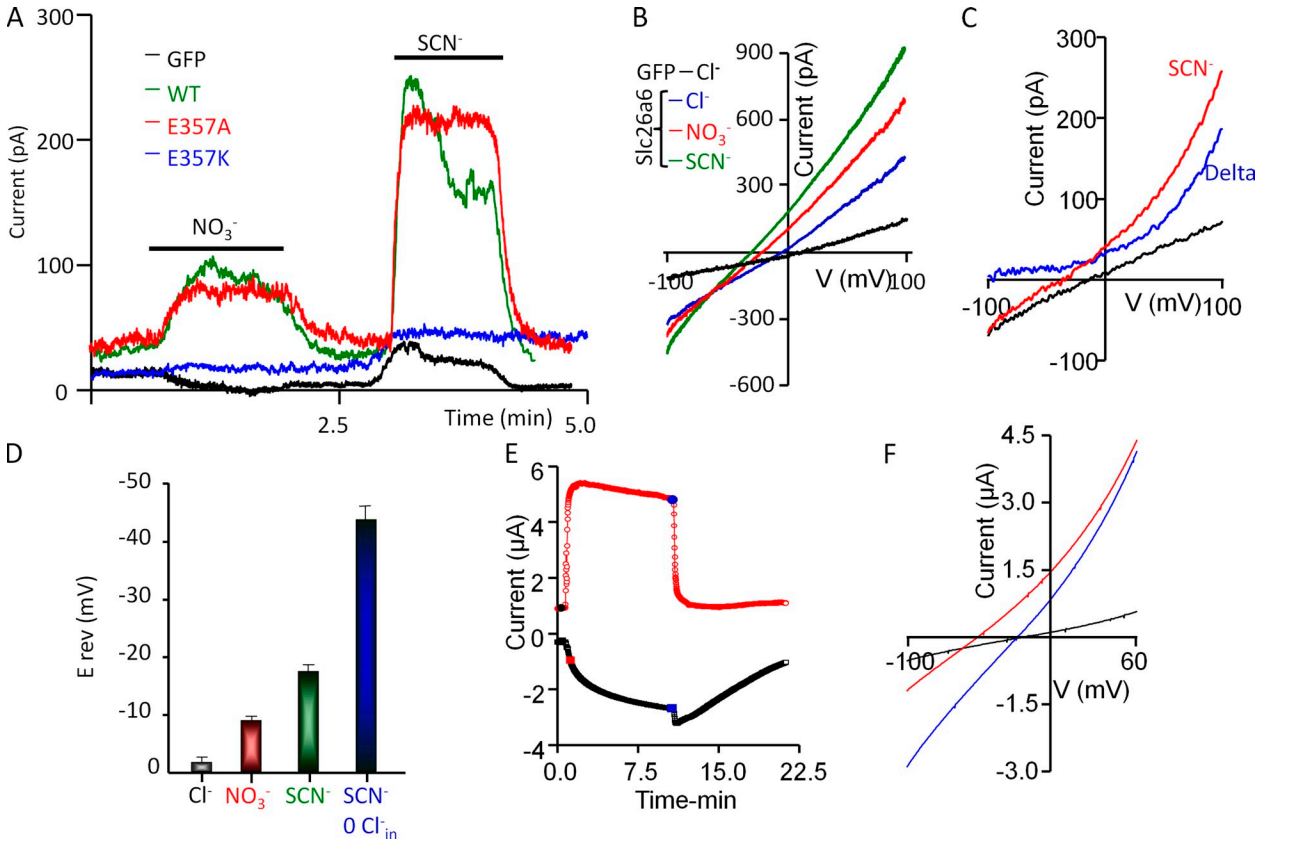

Figure 2. Anion currents by Slc26a6 expressed in HEK cells and oocytes. The whole cell current was measured with HEK cells expressing Slc26a6 or the indicated Slc26a6 mutants and with pipette solution containing 142 mM Cl^- (A and B) or 140 mM Glu^- (C). In A, the membrane potential was clamped at 0 mV, and current recording was begun at bath solution containing 149 mM Cl^-. Where indicated, bath solution was changed to Cl^--free solution containing 145 mM NO_3^- or 145 mM SCN^-. To obtain the I-Vs in B and C, current was recorded by 100 msec RAMPs of -100 to 100 mV. The GFP traces are from cells transfected with GFP only. All other traces are from cells transfected with Slc26a6. (D) The mean ± SEM of three to five experiments. (E) The time course of SCN^- current was measured in oocytes expressing Slc26a6 by 100 msec RAMPs of -100 to 100 mV every second. The current at -100 and +60 mV is plotted. The I-Vs in F are from the times indicated by large filled symbols in E. Similar results were obtained in eight experiments.

can mediate electroneutral formate$^-$/Cl$^-$ exchange; and (c) it conducts NO_3^- and SCN$^-$ (and Cl$^-$; see Fig. S1 A and Shcheynikov et al., 2006) in a channel-like mode to generate a current, which is best resolved with NO_3^- and SCN$^-$.

A conserved Glu$^-$ in the conductive pathway of SLC26 transporters

Simultaneous functioning in coupled and conductive modes is unusual for any transporter. A key question is whether the same transport pathway mediates both functions. To identify residues that affect the Slc26a6 ion-conductive pathway and structural motifs that control the diverse transport modes of Slc26a6, we used an approach that combines in silico modeling of Slc26a6 together with functional assays. To develop the Slc26a6 model, the mouse Slc26a6 protein sequence was submitted to the 3D-Jury metaserver using default settings (Ginalski et al., 2003). The 3D-Jury software uses the PSIPRED secondary structure prediction software to predict the location of α helices within the Slc26a6 sequence (Fig. S2 A). We focused on the region encompassing residues 41–440, which includes 13 helices. The graphical output of PSIPRED describes the confidence of prediction (conf), predicted secondary structure (pred), and target sequence (AA). In parallel, the TopPred II software was used to describe the 2-D transmembrane spans of Slc26a6 (Fig. S2 B). TopPred II used the Kyte-Doolittle hydrophobicity scale to generate several models. All models that indicated intracellular N and C terminals, as was reported previously for Slc26a6 (Lohi et al., 2003), predicted 12 TMDs.

The Slc26a6 TMD sequence was then further analyzed by the 3D-Jury for structural similarity to other proteins. The predicted similarity of the top seven proteins, which received a slightly higher Jscore (51.83–54.83) than the

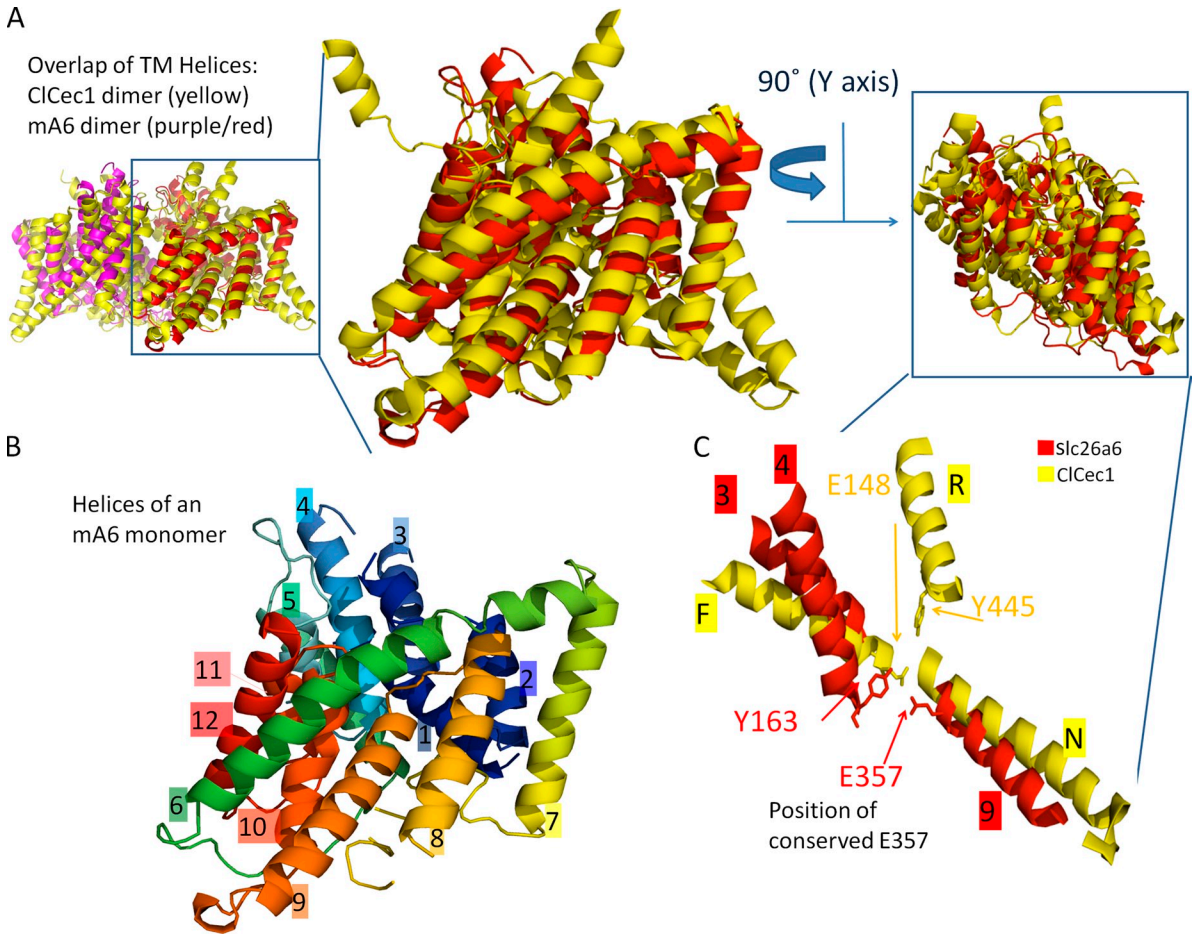

Figure 3. The putative structural model of the Slc26a6 TMDs is similar to the resolved CLC-ec1 TMDs. The putative structure of slc26a6 TMDs was predicted using the 3D-Jury software. (A) The PyMol software was used to generate the model of Slc26a6 TMDs (red/purple) and an overlap with CLC-ec1 crystal structure (yellow). The image on the left shows the dimer configuration, the middle is a magnified image of the TMDs, and the right image is a 90° rotation about the vertical axis. This analysis depicts the high similarity between the TMDs of the two proteins. (B) The predicted position of the Slc26a6 TMD helices. (C) A region within the Slc26a6 TMDs, with a spatial architecture similar to the CLC-ec1 ion-gating domain. The Slc26a6 Y163 and E357 (red) had a putative orientation similar to the CLC-ec1 E148 and Y445 (yellow) that were shown to coordinate Cl$^-$ binding (Dutzler et al., 2002). Note that the two sites do not fully overlap because they are located in opposite sides of the inverted repeat structures.

eighth (51.50), is clustered at the STAS domain at the C terminus of Slc26a6. This domain has a high predicted structural similarity to the SpoIIAA protein (Aravind and Koonin, 2000) and for the solved structure of the Slc26a5 STAS domain (Pasqualetto et al., 2010). These similarities were also predicted by 3D-Jury. The eighth protein predicted by 3D-Jury with high structural similarity to the TMDs of Slc26a6 is the Cl^- transporter CLC-ec1. We reasoned that this similarity should be more relevant for identifying the Slc26a6 ion transport mechanism.

The analysis above led us to focus on the CLC proteins because the structure of CLC-ec1 (Dutzler et al., 2002) and now of a eukaryotic CLC (Feng et al., 2010) is available, and because members of both the CLC and SLC26 transporters can function as coupled and uncoupled transporters (Miller, 2006). The 3D-Jury program was then used to predict a 3-D model of the Slc26a6 TMDs based on the tertiary structural similarity to CLC-ec1. The Slc26a6 TMDs fold (purple/red in Fig. 3, A and B) and the overlap with CLC-ec1 were then generated with PyMol software. Fig. 3 A shows the highly similarly predicted fold of the Slc26a6 and CLC-ec1 TMDs (deposited in the Protein Data Bank under accession no. 2FEE). Further analysis of the models shown in Fig. 3 C revealed a region within the TMDs of the Slc26a6, with a spatial architecture similar to the CLC-ec1 ion-conducting/-gating domain. Moreover, Slc26a6 residues Y163 and E357 (Fig. 3 C, red) are predicted to have an orientation similar to CLC-ec1 residues Y445 and E148 (Fig. 3 C, yellow), which were shown to coordinate Cl^- ion binding (Dutzler et al., 2002). Note that the two sites do not fully overlap because they are located in opposite sides of the inverted repeat structures. The mutation E148A in CLC-ec1 eliminated the coupled $2Cl^-/H^+$ exchange and resulted in uncoupled Cl^-

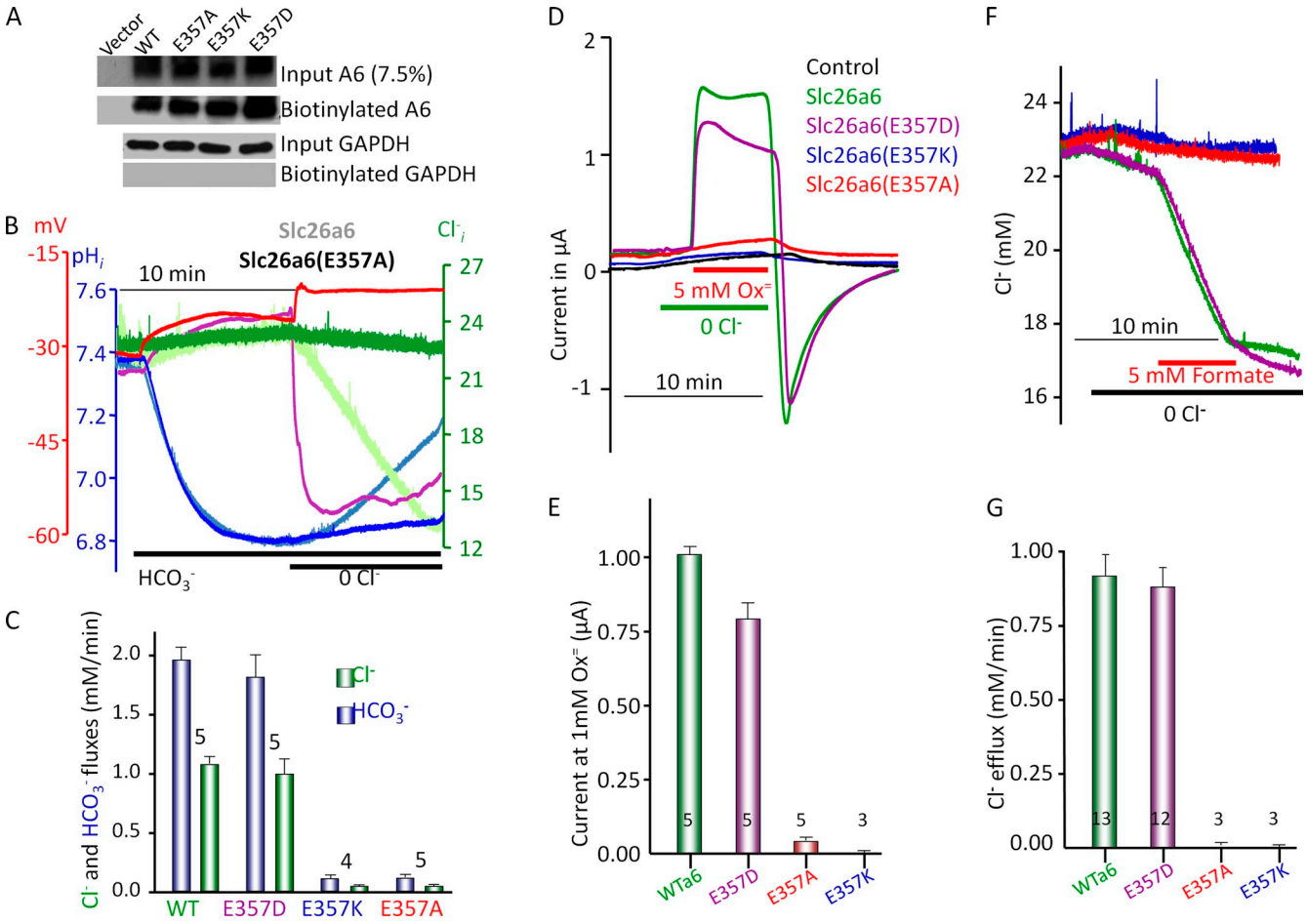

Figure 4. E357 is crucial for all forms of Cl^--coupled exchange by Slc26a6. (A) Surface expression of Slc26a6 mutants expressed in HEK cells. The expression of the cytoplasmic GAPDH serves as loading and biotinylation controls. (B) Example traces of Cl^-_i (green), pH_i (blue), and membrane potential (red) measured in oocytes expressing Slc26a6(E357A). (C) The summary of flux rates measured with Slc26a6, Slc26a6(E357D), Slc26a6(E357A), and Slc26a6(E357K). (D) Individual traces and (E) the summary of oxalate current as a result of $oxalate^=/Cl^-_i$ exchange mediated by the indicated Slc26a6 mutants measured in the absence of Cl^-_o and the presence of 5 mM bath $oxalate^=$. (F) Individual traces and (G) the summary of Cl^-_i/$formate^-$ exchange by the indicated Slc26a6 mutants, measured as $formate^-$-driven Cl^- efflux. Results in summaries are given as mean ± SEM of the number of experiments listed in the columns.

current (Accardi and Miller, 2004). Very recent, similar analysis of the eukaryotic CLC showed the orientation and role of the equivalent Glu^- (E210) (Feng et al., 2010). We reasoned that E357 in Slc26a6 may have a similar function. Further analysis showed that the Glu^- identified by the structural modeling is highly conserved in all SLC26 transporters and across species, with only a conserved E/D substitution in SLC26A8 (Fig. S3). This further suggests that the Glu^- might be of functional importance.

Slc26a6 E357 differentiates between coupled and uncoupled transport

To test the role of E357 in Slc26a6, it was mutated to aspartate, a conserved substitution that preserves the negative charge, to K in which the charge was switched from negative to positive, and to A that neutralizes the charge. The biotinylation assay in Fig. 4 A shows that surface expression of the mutants was not reduced and even slightly increased compared with wild-type Slc26a6.

Reversing the charge resulted in the inhibition of all Slc26a6-mediated transport functions. Thus, E357K showed no Cl^-/HCO_3^- (Fig. 4 C) or $formate^-/Cl^-$ (Fig. 4, F and G) exchange. In Fig. 4 (D and E), $oxalate^=$ transport was evaluated by measuring the Cl^--dependent $oxalate^=$ current, which was completely inhibited by E357K mutation. Slc26a6(E357K) also showed almost no NO_3^- and SCN^- currents when expressed in HEK cells (Fig. 2) or *Xenopus* oocytes (Fig. 5), nor a change in membrane potential upon the removal of Cl^-_o (not depicted). On the other hand, the conserved E357D mutation had no effect on Cl^-/HCO_3^- exchange (Fig. 4 C) and $formate^-/Cl^-$ exchange (Fig. 4, F and G), slightly

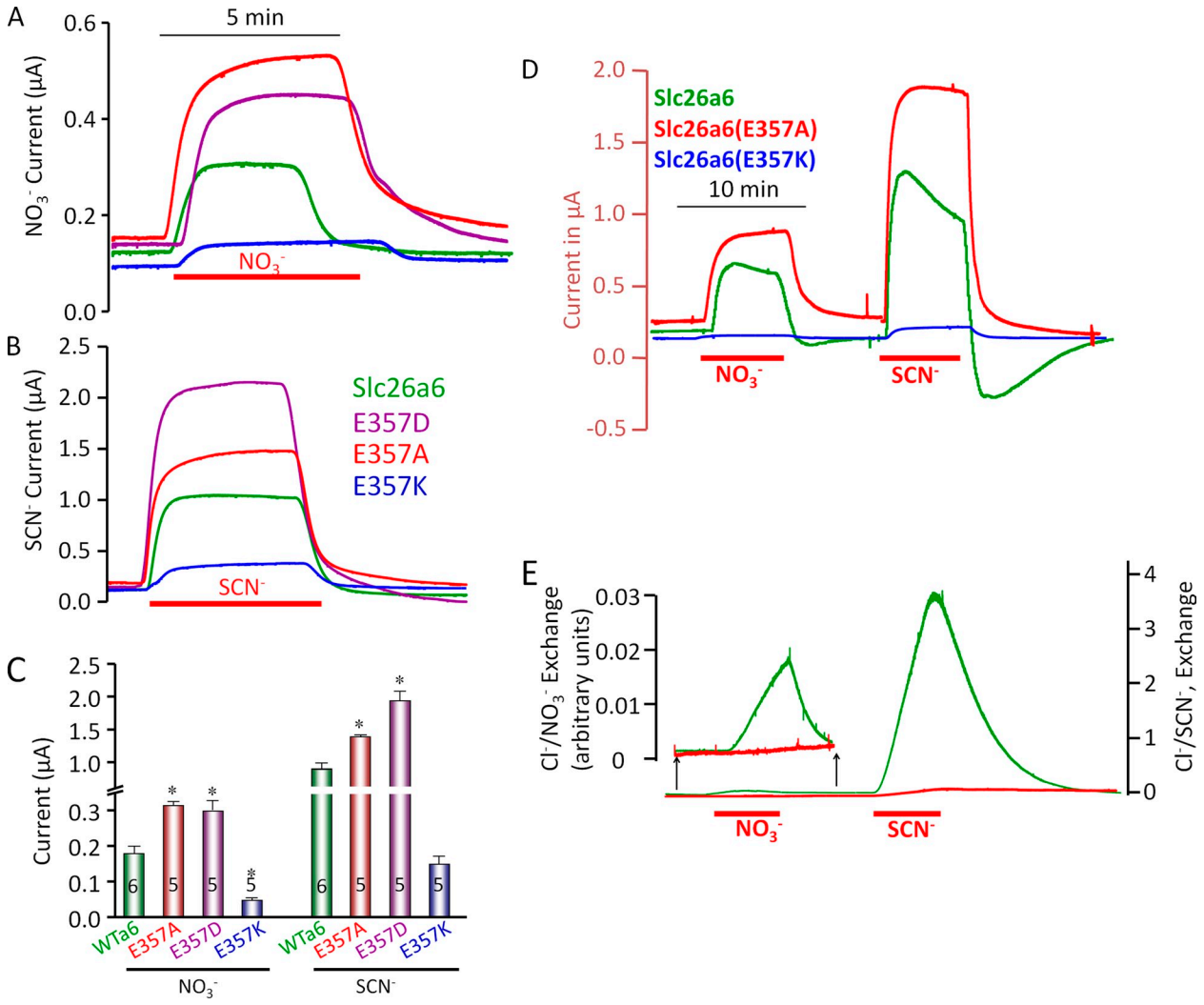

Figure 5. E357 differentiates coupled and uncoupled transport by Slc26a6. Current by wild-type or the indicated slc26a6 mutants was measured in oocytes clamped at 0 mV. NO_3^- and SCN^- currents were measured by replacing bath Cl^- with these anions. (A–C) Individual traces and the summary of the currents. Current and intracellular NO_3^- or SCN^- (D and E) were measured by Slc26a6 and the indicated mutants. For simplicity, the current traces are not shown for E, but they were similar to those in D. Results similar to those in D and E were obtained in four experiments, and the results in C are the mean ± SEM of the indicated number of experiments.

reduced oxalate$^{=}$/Cl^- exchange (Fig. 4, D and E), and modestly, but significantly, increased the NO3$^-$ and SCN^- currents (Fig. 5, A–C). In addition, E357D had no effect on the stoichiometry or the coupling of any of the transport modes. The findings with E357K and E357D indicate that the absence of a positive charge in position 357 is crucial for all forms of transport by Slc26a6. Moreover, by analogy with CLC-ec1 and the eukaryotic CLC, the present findings suggest that the transport of all anions by Slc26a6 share a pathway where Glu^- at positions 357 and 220, respectively, act as gating residues.

The most significant results were obtained with Slc26a6(E357A). This mutation eliminated all forms of coupled transport while sparing and increasing the uncoupled current by Slc26a6. Fig. 4 shows that Slc26a6 (E357A) does not mediate Cl^-/HCO_3^- exchange (Fig. 4, B and C), Cl^--coupled oxalate$^{=}$ (Fig. 4, D and E), and formate$^-$ transport (Fig. 4, F and G). In contrast, Figs. 2 and 5 (A–C) show that NO_3^- and SCN^- currents are not affected or are increased by the E357A mutation. Because Slc26a6 can mediate small Cl^-/NO_3^- and Cl^-/SCN^- exchange, coupled and uncoupled transport can be measured simultaneously in the same cell. In Fig. 5 (D and E), replacing Cl^-_o with NO_3^- or SCN^- in oocytes expressing wild-type Slc26a6 and bathed in HEPES-buffered medium resulted in a large current. As a control, the E357K mutation inhibited all transport modes. The resin used to measure Cl^- is ~10 times more sensitive to NO_3^- and 1,000 times more sensitive to SCN^- (not depicted) and was thus used to measure the net transport of these ions. Fig. 5 E shows that the E357A mutation eliminated the Cl^-/NO_3^- (inset) and Cl^-/SCN^- exchange.

The combined results with Slc26a6 indicate that Glu^- at position 357 is involved in ion flux through the conductive pathway and plays a role in determining the slc26a6 functional mode. Thus, Glu^- that is at the same predicted position in Slc26a6 and CLC transporters appears to have a similar function to determine the mode of passage of the anions through the transport pathway.

Slc26a3 E367 differentiates between coupled and uncoupled transport

Another SLC26 transporter that mediates simultaneously both coupled and uncoupled anion transport is Slc26a3 (Shcheynikov et al., 2006). Extending our study to Slc26a3 offered the opportunity to test the generality of the role of the conserved Glu^- (Fig. S3) in determining transport properties and gating. We analyzed the effects of the corresponding Glu^- mutations, E367A and E367K, on Slc26a3 activity. The expression of wild-type Slc26a3 results in lower steady-state pH_i because of constitutive Cl^-/OH^- exchange (Shcheynikov et al., 2006). Expressing the E367A and E367K Slc26a3 mutants in oocytes resulted in higher steady-state pH_i (~7.1 and 7.3, respectively; Fig. 6 A). Perfusing the oocytes with HCO_3^--buffered medium reduced pH_i to the same level in all oocytes. Mutation of the conserved Glu^- to lysine (E367K) completely inhibited Slc26a3 activity, as was found for Slc26a6 (Fig. 4). On the other hand, the E367A mutation inhibited Slc26a3 Cl^-/HCO_3^- exchange activity by ~60%. More importantly, the E367A mutation changed the residual Cl^- and HCO_3^- flux ratio from 2:1 to 1:1. The $2Cl^-/1HCO_3^-$ stoichiometry likely involves the flow of two Cl^- molecules and one HCO_3^- molecule through the transport pathway in each

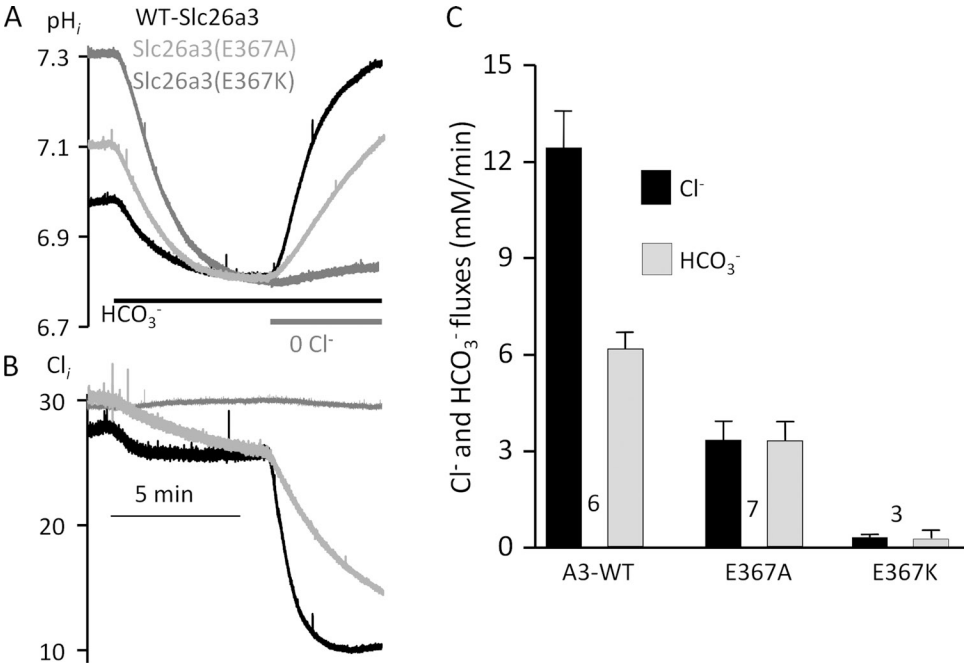

Figure 6. E367 is essential for Cl^-/HCO_3^- exchange by Slc26a3. (A and B) Individual traces and (C) the mean ± SEM of Slc26a3-mediated Cl^-/HCO_3^- exchange measured in oocytes expressing Slc26a3, Slc26a3(E367A), and Slc26a3(E367K). Note that the E367K mutation eliminates the exchange, whereas the E367A mutation markedly inhibited the exchange while changing the stoichiometry of the residual Cl^- and HCO_3^- fluxes from 2:1 to 1:1.

turnover cycle. Neutralizing the Glu^- charge did not prevent accommodating the Cl^- and HCO_3^- by the conduction pathway, but it apparently dissociated their flow to result in a $1Cl^-/1HCO_3^-$ stoichiometry. The conserved Glu^- was also mutated in the electroneutral SLC26A4. In this case, mutating the Glu^- to lysine or alanine eliminated Cl^-/HCO_3^- exchange by SLC26A4 (not depicted). Hence, the conserved Glu^- determines the mode of ion flow through the SLC26 transporters.

Because Slc26a3 also shows uncoupled current, generating large Cl^-, NO_3^-, and SCN^- currents (Shcheynikov et al., 2006), we were able to further examine the effect of the Glu^- mutants on current by Slc26a3. Fig. 7 C shows that Slc26a3(E367K) does not conduct current with any of the anions. In contrast, the Slc26a3(E367A)-mediated Cl^-, NO_3^-, and SCN^- currents are similar to the currents mediated by the wild-type Slc26a3 (Fig. 7, A–C). In addition, the E367A mutation had no effect on the reversal potential for NO_3^- and SCN^-, but it did change the reversal potential for Cl^- (see Fig. 7 I). To further explore the effect of the E367A mutation, we measured simultaneously the membrane potential and ion fluxes. Fig. 7 D shows that in Slc26a3-expressed oocytes, replacing Cl^-_o with gluconate (0 Cl^-) resulted in a slow Cl^- efflux, and replacing Cl^-_o with NO_3^- resulted in NO_3^- influx, which has been previously shown to be a result of Cl^-/OH^- and Cl^-/NO_3^- exchange, respectively (Shcheynikov et al., 2006). Similarly, replacing Cl^-_o with SCN^- resulted in SCN^- influx (Fig. 7 F) as a result of Cl^-/SCN^- exchange. The E367A mutation markedly reduced Cl^-, NO_3^-, and SCN^- fluxes. The Cl^- fluxes are mediated by $2Cl^-/1OH^-$ exchange (Ko et al., 2002), and the inhibition of these fluxes resulted in the reduction of the associated changes in the membrane potential (Fig. 7, E and I). Because the NO_3^- and SCN^- currents are mostly the result of uncoupled transport, the E367A mutation had no measurable effect on the change in membrane potential observed by replacing Cl^-_o with these anions (Fig. 7, E, G, and I). Hence, the E367A mutation markedly inhibited coupled fluxes, changed the stoichiometry of the residual fluxes from $2Cl^-/1HCO_3^-$ to $1Cl^-/1HCO_3^-$, and had no effect on the uncoupled current fluxes.

DISCUSSION

Ion transport by exchangers, cotransporters, and pumps is usually tightly coupled and proceeds along a defined turnover cycle, although a small uncoupled transport can be measured as a slippage mode of transport (for example, see Knauf et al., 1977; Grygorczyk et al., 1987). Two noted exceptions that do not follow this rule are several neurotransmitter transporters (Kanner and Borre, 2002; Torres and Amara, 2007) and members of the CLC Cl^- transporters (Miller, 2006). A third example is described here with Slc26a3 and Slc26a6. Although the SLC26 transporter primary sequence has minimal identity with CLC-ec1, the predicted structure of the SLC26 transporter TMDs is most similar to the CLC transporters and so are the ions they transport. Low primary sequence similarity, but close structural similarity, is not unprecedented. As was previously demonstrated for the Na^+/galactose cotransporter, the primary sequence cannot be the only criteria in determining similarity in structure. Hence, the crystal structures of Na^+/galactose cotransporter and of the Na^+/neurotransmitter symporter LeuT are highly similar, in spite of their limited primary sequence similarity (Faham et al., 2008). Moreover, the CLC-ec1 and the eukaryotic CLC show <25% primary sequence similarity but very high structural similarity (Feng et al., 2010).

The data obtained from the structural analysis for the SLC26 transporters provided substantial information about the conserved Glu^- in the SLC26 transporters. This information was helpful in correlating functional importance of the conserved Glu^- with other similar transporters. In the case of the SLC26 and CLC transporters, both can function as coupled and uncoupled transporters. However, a key difference between the CLC and SLC26 transporters is that the CLC transporters function either as coupled $2Cl^-/H^+$ exchangers or mediate uncoupled Cl^- (Dutzler et al., 2003; Accardi and Miller, 2004; Accardi et al., 2005; Walden et al., 2007), NO_3^-, and SCN^- (Hebeisen et al., 2003; Bergsdorf et al., 2009; Zifarelli and Pusch, 2009) current, with ion conduction requiring neutralization of the conserved Glu^-. On the other hand, in the presence of Cl^- and HCO_3^-, the SLC26 transporters function as a strictly electrogenic coupled Cl^-/HCO_3^- exchanger with distinct isoform stoichiometry (Ko et al., 2002; Shcheynikov et al., 2006), whereas in the absence of HCO_3^-, they conduct Cl^- (Fig. S1 A). In the presence of NO_3^- and SCN^-, and the absence and presence of HCO_3^-, the SLC26 transporters mediate modest Cl^-/NO_3^-, HCO_3^-/NO_3^-, Cl^-/SCN^-, and perhaps HCO_3^-/SCN^- exchange, but mostly conduct NO_3^- and SCN^-. Hence, the SLC26 transporters are unique in that under normal physiological conditions, a large fraction of the turnovers results with uncoupled flux of one ion in a channel-like mode, which is higher with $SCN^- > NO_3^- > Cl^-$, whereas other turnovers are a result of fully coupled transport.

Coupled and uncoupled transport by the same transporter is energetically unfavorable, and the SLC26 transporters must benefit from the investment of the osmotic (gradient) energy to function in this mode. Two such advantages can be regulation of the extent of net flux and of the membrane potential in their microdomain. Under physiological conditions when Cl^- and HCO_3^- (Slc26a3 and Slc26a6), $formate^-$, $oxalate^=$, and other carboxylic acids (Slc26a6) are the dominant

anions, adjusting the extent of coupled and uncoupled transport can be used to adjust the extent of HCO_3^- and carboxylic acid absorption. Luminal membrane hyperpolarization by the uncoupled transport can modulate fluxes by Slc26a3 and Slc26a6. Other advantages for coupled and uncoupled transport by the same transporter likely exist, and further work is needed to uncover them.

Successful design is usually conserved in nature and can be found in several proteins of diverse function. This seems to be the case for the CLC and SLC26 transporter conductive pathway. In CLC-ec1, the Cl^- path is gated by Glu^- 148 and tyrosine 445 that are contributed by two helices (Dutzler et al., 2003). Similarly, in the eukaryotic CLC, Glu^- 210 and tyrosine 515 gate the Cl^- path (Feng et al., 2010). Mutation of the conserved Glu^- eliminates the transport of the H^+ that is coupled to the transport of $2Cl^-$, while sparing and augmenting the uncoupled transport of Cl^- (Accardi et al., 2004; Walden et al., 2007; Feng et al., 2010). Mutation of the tyrosine results in variable uncoupling, depending on the residue that substitutes for tyrosine in position 445

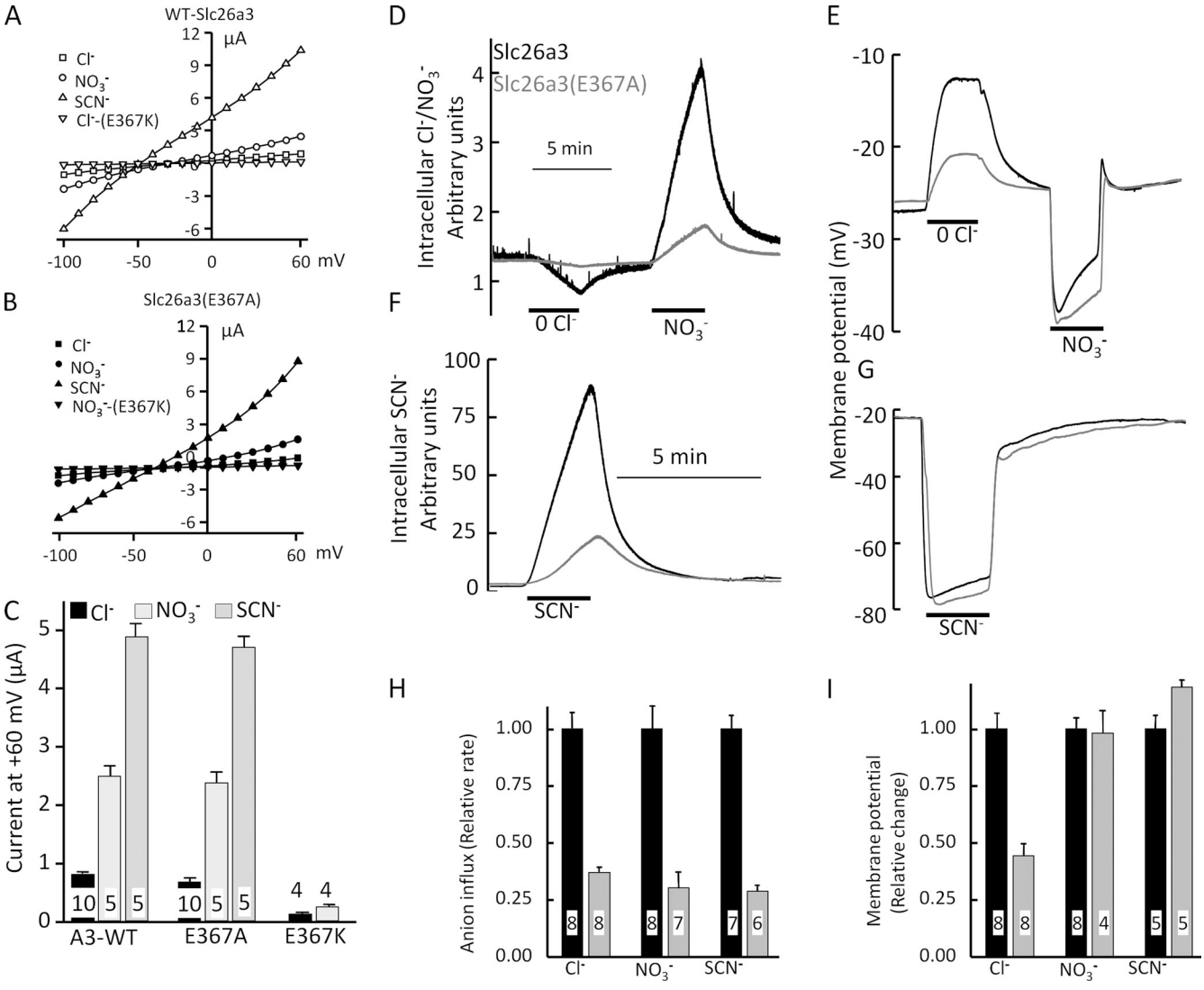

Figure 7. Slc26a3 current is retained by Slc26a3(E367A). Cl^-, NO_3^-, and SCN^- (A–C) current by Slc26a3 and mutants was measured by a step protocol between −100 and +60 mV at 10-mV intervals from a holding potential of 0 mV. To obtain the I-V curves, oocyte bath in ND96 was perfused with ND96, and I-Vs were collected every minute for 5–10 min. The medium was then changed to a NO_3^--based medium, and I-Vs were recorded for 5–10 min. The bath solution was returned to ND96 until recovery of the basal Cl^- current. Finally, the solution was changed to the SCN^--based solution, and I-Vs were collected for 5–10 min. The I-V curves shown were obtained 5 min after the solution changes. Simultaneous measurement of Cl^-/NO_3^- exchange (D) and the associated change in membrane potential (E), and Cl^-/SCN^- exchange (F) and the associated change in membrane potential (G) were measured with Slc26a3 (dark traces and columns) and Slc26a3(E367A) (gray traces and columns). As indicated, the oocytes were perfused with ND96 (Cl^--containing) and then with the NO_3^-- or SCN^--based solutions. The mean ± SEM of the ion flux rates (H) and associated changes in membrane potential (I) are given for the indicated number of experiments.

(Walden et al., 2007). In silico analysis showed that the structure of the TMDs of SLC26 transporters is predicted to be most similar to that of the CLC transporters. Moreover, the predicted SLC26 transporter ion pathway poses a conserved Glu^- and a tyrosine, and the Glu^- is conserved in all SLC26 transporters in species from invertebrates to humans. It is clear that the conserved Glu^- is essential for the transport because reversing the charge in this position inhibited all forms of transport by Slc26a3, Slc26a6, and Slc26a4 (unpublished data for the latter). On the other hand, neutralization of the charge inhibited all forms of the coupled exchange while sparing the uncoupled transport. It is possible that neutralizing the negative charge of the conserved Glu^- residue has a similar effect to that proposed for the CLC transporters, where an additional Cl^- ion was observed in the ion conductance pathway of CLC-ec1, which carries the E148Q mutation (Dutzler et al., 2003).

An alternative explanation for the simultaneous coupled and uncoupled anion flux by the same transporters as in the case of Slc26a3 and Slc26a6 may relate to the ionic radii and hydration energies of the anions that affect their flow through the conduction pathway. It is possible that HCO_3^- (or CO_3^{-2}) flow through the transporters is hindered by the conserved Glu^- and requires the energy of the Cl^- gradient to induce a conformational change that determines the orientation of the conductive pathway to allow access of HCO_3^- to either side of the membrane. On the other hand, the flow of Cl^-, NO_3^-, and SCN^- is not hindered by the conserved Glu^- to allow their flow in a channel-like mode.

This work was supported by National Institutes of Health (grants DE12309 and DK076638). E. Ohana was supported in part by the Machiah Fellowship (grant 2008-0702) awarded through the Machiah Foundation, a supporting foundation of the Jewish Community Federation of San Francisco, the Peninsula, Marin, and Sonoma Counties.

Lawrence G. Palmer served as editor.

Submitted: 7 September 2010
Accepted: 18 January 2011

REFERENCES

Accardi, A., and C. Miller. 2004. Secondary active transport mediated by a prokaryotic homologue of ClC Cl- channels. *Nature.* 427:803–807. doi:10.1038/nature02314

Accardi, A., L. Kolmakova-Partensky, C. Williams, and C. Miller. 2004. Ionic currents mediated by a prokaryotic homologue of CLC Cl^- channels. *J. Gen. Physiol.* 123:109–119. doi:10.1085/jgp.200308935

Accardi, A., M. Walden, W. Nguitragool, H. Jayaram, C. Williams, and C. Miller. 2005. Separate ion pathways in a Cl^-/H^+ exchanger. *J. Gen. Physiol.* 126:563–570. doi:10.1085/jgp.200509417

Allen, A., G. Flemström, A. Garner, and E. Kivilaakso. 1993. Gastroduodenal mucosal protection. *Physiol. Rev.* 73:823–857.

Almståhl, A., and M. Wikström. 2003. Electrolytes in stimulated whole saliva in individuals with hyposalivation of different origins. *Arch. Oral Biol.* 48:337–344. doi:10.1016/S0003-9969(02)00200-5

Aravind, L., and E.V. Koonin. 2000. The STAS domain—a link between anion transporters and antisigma-factor antagonists. *Curr. Biol.* 10:R53–R55. doi:10.1016/S0960-9822(00)00335-3

Baron, J.H. 2000. The pancreas. *Mt. Sinai J. Med.* 67:68–75.

Bergsdorf, E.Y., A.A. Zdebik, and T.J. Jentsch. 2009. Residues important for nitrate/proton coupling in plant and mammalian CLC transporters. *J. Biol. Chem.* 284:11184–11193. doi:10.1074/jbc.M901170200

Boron, W.F. 2004. Regulation of intracellular pH. *Adv. Physiol. Educ.* 28:160–179. doi:10.1152/advan.00045.2004

Casey, J.R., S. Grinstein, and J. Orlowski. 2010. Sensors and regulators of intracellular pH. *Nat. Rev. Mol. Cell Biol.* 11:50–61. doi:10.1038/nrm2820

Dorwart, M.R., N. Shcheynikov, D. Yang, and S. Muallem. 2008. The solute carrier 26 family of proteins in epithelial ion transport. *Physiology (Bethesda).* 23:104–114.

Durie, P.R. 1989. The pathophysiology of the pancreatic defect in cystic fibrosis. *Acta Paediatr. Scand. Suppl.* 363:41–44.

Dutzler, R., E.B. Campbell, M. Cadene, B.T. Chait, and R. MacKinnon. 2002. X-ray structure of a ClC chloride channel at 3.0 A reveals the molecular basis of anion selectivity. *Nature.* 415:287–294. doi:10.1038/415287a

Dutzler, R., E.B. Campbell, and R. MacKinnon. 2003. Gating the selectivity filter in ClC chloride channels. *Science.* 300:108–112. doi:10.1126/science.1082708

Everett, L.A., B. Glaser, J.C. Beck, J.R. Idol, A. Buchs, M. Heyman, F. Adawi, E. Hazani, E. Nassir, A.D. Baxevanis, et al. 1997. Pendred syndrome is caused by mutations in a putative sulphate transporter gene (PDS). *Nat. Genet.* 17:411–422. doi:10.1038/ng1297-411

Faham, S., A. Watanabe, G.M. Besserer, D. Cascio, A. Specht, B.A. Hirayama, E.M. Wright, and J. Abramson. 2008. The crystal structure of a sodium galactose transporter reveals mechanistic insights into Na+/sugar symport. *Science.* 321:810–814. doi:10.1126/science.1160406

Feng, L., E.B. Campbell, Y. Hsiung, and R. MacKinnon. 2010. Structure of a eukaryotic CLC transporter defines an intermediate state in the transport cycle. *Science.* 330:635–641. doi:10.1126/science.1195230

Ginalski, K., A. Elofsson, D. Fischer, and L. Rychlewski. 2003. 3D-Jury: a simple approach to improve protein structure predictions. *Bioinformatics.* 19:1015–1018. doi:10.1093/bioinformatics/btg124

Grygorczyk, R., W. Schwarz, and H. Passow. 1987. Potential dependence of the "electrically silent" anion exchange across the plasma membrane of Xenopus oocytes mediated by the band-3 protein of mouse red blood cells. *J. Membr. Biol.* 99:127–136. doi:10.1007/BF01871232

Hebeisen, S., H. Heidtmann, D. Cosmelli, C. Gonzalez, B. Poser, R. Latorre, O. Alvarez, and C. Fahlke. 2003. Anion permeation in human ClC-4 channels. *Biophys. J.* 84:2306–2318. doi:10.1016/S0006-3495(03)75036-X

Höglund, P., S. Haila, J. Socha, L. Tomaszewski, U. Saarialho-Kere, M.L. Karjalainen-Lindsberg, K. Airola, C. Holmberg, A. de la Chapelle, and J. Kere. 1996. Mutations of the Down-regulated in adenoma (DRA) gene cause congenital chloride diarrhoea. *Nat. Genet.* 14:316–319. doi:10.1038/ng1196-316

Holm, L., and C. Sander. 1991. Database algorithm for generating protein backbone and side-chain co-ordinates from a C alpha trace application to model building and detection of co-ordinate errors. *J. Mol. Biol.* 218:183–194. doi:10.1016/0022-2836(91)90883-8

Jentsch, T.J. 2008. CLC chloride channels and transporters: from genes to protein structure, pathology and physiology. *Crit. Rev. Biochem. Mol. Biol.* 43:3–36. doi:10.1080/10409230701829110

Jiang, Z., I.I. Grichtchenko, W.F. Boron, and P.S. Aronson. 2002. Specificity of anion exchange mediated by mouse Slc26a6. *J. Biol. Chem.* 277:33963–33967. doi:10.1074/jbc.M202660200

Jiang, Z., J.R. Asplin, A.P. Evan, V.M. Rajendran, H. Velazquez, T.P. Nottoli, H.J. Binder, and P.S. Aronson. 2006. Calcium oxalate urolithiasis in mice lacking anion transporter Slc26a6. *Nat. Genet.* 38:474–478. doi:10.1038/ng1762

Kanner, B.I., and L. Borre. 2002. The dual-function glutamate transporters: structure and molecular characterisation of the substrate-binding sites. *Biochim. Biophys. Acta.* 1555:92–95. doi:10.1016/S0005-2728(02)00260-8

Knauf, P.A., G.F. Fuhrmann, S. Rothstein, and A. Rothstein. 1977. The relationship between anion exchange and net anion flow across the human red blood cell membrane. *J. Gen. Physiol.* 69:363–386. doi:10.1085/jgp.69.3.363

Knauf, F., C.L. Yang, R.B. Thomson, S.A. Mentone, G. Giebisch, and P.S. Aronson. 2001. Identification of a chloride-formate exchanger expressed on the brush border membrane of renal proximal tubule cells. *Proc. Natl. Acad. Sci. USA.* 98:9425–9430. doi:10.1073/pnas.141241098

Ko, S.B., N. Shcheynikov, J.Y. Choi, X. Luo, K. Ishibashi, P.J. Thomas, J.Y. Kim, K.H. Kim, M.G. Lee, S. Naruse, and S. Muallem. 2002. A molecular mechanism for aberrant CFTR-dependent HCO(3)(-) transport in cystic fibrosis. *EMBO J.* 21:5662–5672. doi:10.1093/emboj/cdf580

Ko, S.B., N. Mizuno, Y. Yatabe, T. Yoshikawa, H. Ishiguro, A. Yamamoto, S. Azuma, S. Naruse, K. Yamao, S. Muallem, and H. Goto. 2010. Corticosteroids correct aberrant CFTR localization in the duct and regenerate acinar cells in autoimmune pancreatitis. *Gastroenterology.* 138:1988–1996. doi:10.1053/j.gastro.2010.01.001

Lohi, H., G. Lamprecht, D. Markovich, A. Heil, M. Kujala, U. Seidler, and J. Kere. 2003. Isoforms of SLC26A6 mediate anion transport and have functional PDZ interaction domains. *Am. J. Physiol. Cell Physiol.* 284:C769–C779.

Matsuda, J.J., M.S. Filali, K.A. Volk, M.M. Collins, J.G. Moreland, and F.S. Lamb. 2008. Overexpression of CLC-3 in HEK293T cells yields novel currents that are pH dependent. *Am. J. Physiol. Cell Physiol.* 294:C251–C262. doi:10.1152/ajpcell.00338.2007

Miller, C. 2006. ClC chloride channels viewed through a transporter lens. *Nature.* 440:484–489. doi:10.1038/nature04713

Pasqualetto, E., R. Aiello, L. Gesiot, G. Bonetto, M. Bellanda, and R. Battistutta. 2010. Structure of the cytosolic portion of the motor protein prestin and functional role of the STAS domain in SLC26/SulP anion transporters. *J. Mol. Biol.* 400:448–462. doi:10.1016/j.jmb.2010.05.013

Picollo, A., and M. Pusch. 2005. Chloride/proton antiporter activity of mammalian CLC proteins ClC-4 and ClC-5. *Nature.* 436:420–423. doi:10.1038/nature03720

Scheel, O., A.A. Zdebik, S. Lourdel, and T.J. Jentsch. 2005. Voltage-dependent electrogenic chloride/proton exchange by endosomal CLC proteins. *Nature.* 436:424–427. doi:10.1038/nature03860

Shcheynikov, N., Y. Wang, M. Park, S.B. Ko, M. Dorwart, S. Naruse, P.J. Thomas, and S. Muallem. 2006. Coupling modes and stoichiometry of $Cl^-/HCO3^-$ exchange by slc26a3 and slc26a6. *J. Gen. Physiol.* 127:511–524. doi:10.1085/jgp.200509392

Shcheynikov, N., D. Yang, Y. Wang, W. Zeng, L.P. Karniski, I. So, S.M. Wall, and S. Muallem. 2008. The Slc26a4 transporter functions as an electroneutral Cl-/I-/HCO3- exchanger: role of Slc26a4 and Slc26a6 in I- and HCO3- secretion and in regulation of CFTR in the parotid duct. *J. Physiol.* 586:3813–3824. doi:10.1113/jphysiol.2008.154468

Torres, G.E., and S.G. Amara. 2007. Glutamate and monoamine transporters: new visions of form and function. *Curr. Opin. Neurobiol.* 17:304–312. doi:10.1016/j.conb.2007.05.002

Walden, M., A. Accardi, F. Wu, C. Xu, C. Williams, and C. Miller. 2007. Uncoupling and turnover in a Cl^-/H^+ exchange transporter. *J. Gen. Physiol.* 129:317–329. doi:10.1085/jgp.200709756

Wall, S.M., and V. Pech. 2008. The interaction of pendrin and the epithelial sodium channel in blood pressure regulation. *Curr. Opin. Nephrol. Hypertens.* 17:18–24. doi:10.1097/MNH.0b013e3282f29086

Wangemann, P., K. Nakaya, T. Wu, R.J. Maganti, E.M. Itza, J.D. Sanneman, D.G. Harbidge, S. Billings, and D.C. Marcus. 2007. Loss of cochlear HCO3- secretion causes deafness via endolymphatic acidification and inhibition of Ca2+ reabsorption in a Pendred syndrome mouse model. *Am. J. Physiol. Renal Physiol.* 292:F1345–F1353. doi:10.1152/ajprenal.00487.2006

Xie, Q., R. Welch, A. Mercado, M.F. Romero, and D.B. Mount. 2002. Molecular characterization of the murine Slc26a6 anion exchanger: functional comparison with Slc26a1. *Am. J. Physiol. Renal Physiol.* 283:F826–F838.

Yang, D., N. Shcheynikov, W. Zeng, E. Ohana, I. So, H. Ando, A. Mizutani, K. Mikoshiba, and S. Muallem. 2009. IRBIT coordinates epithelial fluid and HCO3- secretion by stimulating the transporters pNBC1 and CFTR in the murine pancreatic duct. *J. Clin. Invest.* 119:193–202.

Zifarelli, G., and M. Pusch. 2009. Conversion of the 2 Cl(-)/1 H+ antiporter ClC-5 in a NO3(-)/H+ antiporter by a single point mutation. *EMBO J.* 28:175–182. doi:10.1038/emboj.2008.284